metals

MDPI

Article

Synthesis ZrON Films with Raman-Enhancement Properties Using Microwave Plasma

Arsen Muslimov [1,*], Sergey Antipov [2], Makhach Gadzhiev [2] and Vladimir Kanevsky [1]

[1] Federal Scientific Research Centre "Crystallography and Photonics", Russian Academy of Sciences, Shubnikov Institute of Crystallography, 119333 Moscow, Russia
[2] Joint Institute for High Temperatures, Russian Academy of Sciences, 125412 Moscow, Russia; antipov@ihed.ras.ru (S.A.); makhach@mail.ru (M.G.)
* Correspondence: amuslimov@mail.ru

Abstract: The paper investigates the characteristics of the formation and morphology of microstructured zirconium oxynitride (ZrON) films, taking into account structural polymorphism during the impact of atmospheric-pressure microwave nitrogen plasma with the influx of active oxygen from the surrounding atmosphere. Optical, hydrophobic, Raman-active properties of ZrON films have been studied. X-ray diffractometry (XRD), scanning electron microscopy (SEM), ellipsometry method, and Raman spectroscopy, and moisture-resistance properties are used as analytical research methods. It is shown that during the short-term impact of microwave plasma, a morphologically heterogeneous ZrON film can be formed with a set of microhills with a uniform phase composition along the surface. The phase composition of the ZrON surface corresponds to the monoclinic structure of ZrO_2. In the volume of the film, a predominantly tetragonal structure of ZrO_2 is observed, as well as inclusions of the monoclinic structure of ZrO_2. A mechanism for the formation of a ZrON film, taking into account polymorphism and phase transitions, is proposed. The optical properties of ZrON films are determined by both the dielectric phase of ZrO_2 and the inclusions of the high-conductivity phase of ZrN. A combination of such factors as the developed microrelief and monoclinic surface structure, as well as nitride phase inclusions, enhance the hydrophobic properties of the ZrON film surface. It is shown that the surface hydrophobicity and resonant effects on ZrN inclusions allow for the enhancement of the Raman spectrum intensity due to the high concentration of analyte molecules in the scanning area.

Keywords: films; microwave plasma; zirconium oxide; nitrogen; Raman spectra; microbubbles; microscopy

Citation: Muslimov, A.; Antipov, S.; Gadzhiev, M.; Kanevsky, V. Synthesis ZrON Films with Raman-Enhancement Properties Using Microwave Plasma. *Metals* **2023**, *13*, 1927. https://doi.org/10.3390/met13121927

Academic Editor: Kristián Máthis

Received: 31 October 2023
Revised: 18 November 2023
Accepted: 21 November 2023
Published: 23 November 2023

1. Introduction

Metal oxynitrides (MONs) are a new family of materials in which a fraction of oxygen atoms are replaced with nitrogen atoms. Due to this substitution, the functionality of the materials is expanded, and they acquire new properties. For example, aluminum oxynitride ceramics (AlON) [1,2] are almost twice as hard as sapphire and transparent (≥80%) in a wide range of the electromagnetic spectrum and are used as protective glasses, lenses, etc. Titanium oxynitride (TiON) nanoparticles represent powerful active sites when added to photocatalytic devices, or to electrodes for capacitors, batteries, and fuel cells [3,4]. Due to its unique mechanical properties, silicon oxynitride (SiON) [5,6] has great potential for high-temperature applications as a thermal insulation coating, as well as in electronics and chemical technologies.

In recent decades, an area such as plasmonics, which studies the interaction of light with metallic or heavily doped semiconductor materials and promises revolutionary discoveries in modern photonic technologies, has been actively developing. A separate direction of plasmonics is the control of the propagation of plasmon-polariton waves in the

metal-dielectric system. Metal is necessary for the existence of electronic plasma, and the dielectric allows the linking of electronic plasma with the volumetric light wave. In this regard, composite ceramics of TiON, consisting of the dielectric phase of titanium dioxide and the conductive phase of titanium nitride, are promising and actively researched. For example [7], TiON composite films demonstrate enhanced absorption of laser light above the percolation threshold in the visible and infrared ranges.

Systems close to ZrON in structure and properties, such as ZrN, are also of interest. For instance, ZrN is characterized by reduced dielectric losses compared to TiN, while retaining almost the same conduction electron density, resulting in stronger and blueshifted plasmonic responses compared to TiN. However, a review [8] indicates a scarcity of experimental studies on the plasmonic properties of ZrN, and the activity of plasmonic devices based on ZrN only demonstrates theoretical potential. There are even fewer studies related to ZrON, and this direction is quite relevant. In [9], it is shown that higher nitrogen and oxygen contents can reduce the screened plasma frequency ωc. Interestingly, the bilayer ZrN/ZrON structures with some ZrON thickness are more metallic than ZrN films, which should be reasonable since the mutual diffusion through the ZrN/ZrON interface may cause a ZrON buffer zone with substitute oxygen atoms generating more free carriers.

One of the main drawbacks of ZrO_2 is complex polymorphism [10,11], creating problems during synthesis and operation. In addition to the main transitions, there are several intermediate forms associated with the theoretical prohibition of direct transitions. The low-temperature monoclinic (m)-phase P21/c is considered stable. At temperatures above 1000 °C, a stretched martensitic transformation to the tetragonal (t)-phase P42/nmc is observed, characterized by strong hysteresis and a destructive volume change of 4%. This change is the cause of destruction under thermal cycling conditions. At temperatures above 2370 °C, a transition to the cubic (c)-phase Fm3m is observed. Accordingly, reverse transitions are observed when cooling the ZrO_2 sample. Similar processes can be expected in ZrON with an excess oxide phase content.

The main methods of oxynitride creation are the post-synthesis oxidation of metal nitrides or synthesis in a multi-component gaseous medium (often using an ammonia flow). It appears that plasma synthesis is the most optimal method for the mass production of oxynitride materials. Overall, the analysis of research demonstrates the underestimation of plasma technologies. Previously [12,13], the successful application of low-temperature plasma in the formation of titanium oxynitrides, both in the form of film structures and powder, was shown. Titanium oxynitride samples were obtained using an arc plasmatron with vortex stabilization and an expanding channel. Nitrogen was used as the plasma-forming gas. Plasma treatment was conducted in an open atmosphere [14]. The use of arc plasma proved effective, but a high gas temperature up to 10 kK complicates the treatment control, with a high probability of sample destruction. A more controllable approach is the use of microwave (MW) discharge at atmospheric pressure. Continuous and stable MW discharge at atmospheric pressure is maintained in a dielectric (quartz) tube. High-purity nitrogen is used as the plasma-forming gas. Depending on the output power, the temperature in the axial region of the plasma can reach 5 kK [15]; however, at the open end of the quartz tube, the temperature is significantly lower, and there is a sufficiently high concentration of active oxygen and nitrogen.

In the synthesized ZrON structures, an enhancement of Raman light scattering can be expected due to the plasmonic resonance [16,17] of electrons in ZrN inclusions. A key point is also the possibility of converting the transverse electromagnetic radiation of the laser into a longitudinal plasma mode, which can propagate along the metal-dielectric heteroboundaries in ZrON. Laser radiation on a rough surface interacts with surface plasmons, leading to an increase in energy density in the subsurface layer. Consequently, the amplitude of the electric field of the wave increases, and the signal of Raman scattering is enhanced. The conversion efficiency is determined by the degree of periodicity of the plasmonic lattice (in our case, the model represents a lattice at the nodes of which ZrN

inclusions are concentrated) and the commensurability of the wavelength of plasmon-polaritons with the parameter of the plasmonic lattice.

Certainly, creating a periodic plasmonic lattice with given parameters during plasma treatment is quite challenging, but there is an opportunity to form a high-density microhill structure on the surface. The fact is that during plasma treatment, cavitation bubbles may form [18], which usually hinder uniform treatment. The formation of microhills on the surface of ZrON may have several advantages. During plasma treatment, it is possible to reach the temperatures of phase transitions in ZrON, and the presence of microstructure will help suppress their destructive effects. Moreover, for detecting Raman scattering spectra at ultra-low concentrations of analyte molecules, it is desirable to have hydrophobic substrates that prevent the substance spreading on the surface (preliminary concentration method), leading to a combination of electrodynamic and chemical signal enhancement effects and allowing the registration of a more refined structure of the Raman scattering spectrum of the substance [19]. For ZrO_2, the transition to a hydrophobic state is a problem [20]: there is a tendency for the surface of t-ZrO_2 to transition to a superhydrophilic state with increasing oxygen vacancy concentration. One way to enhance hydrophobicity without using hydrophobic coatings is texture selection and increasing the surface roughness [21]. In this regard, the presence of microhills may enhance the hydrophobic component. Additionally, nitrogen-containing inclusions can enhance hydrophobic properties [12].

This study investigated the features of the formation and morphology of microstructured films of zirconium oxynitride ZrON, considering structural polymorphism during the exposure of microwave nitrogen plasma with an influx of active oxygen from the surrounding atmosphere on metallic Zr films. The optical, hydrophobic, and Raman-active properties of ZrON films were studied.

2. Materials and Methods

A Zirconium (Zr) layer was applied to the sapphire plate. The film was applied by magnetron sputtering. Next, the Zr film was treated using atmospheric-pressure microwave nitrogen plasma. To achieve this, a microwave (MW) plasmatron based on a 2.45-GHz magnetron with a nominal output power of 1.1 kW was used (Figure 1). The design and operating principles of such a plasmatron were discussed in detail in [22,23]. Here, we give only a brief description of it. Plasma was generated in a closed rectangular WR-340 waveguide, operating in H_{10} mode. In the middle of the wide walls of the waveguide's central part, two pipe nozzles were welded coaxially for a gas discharge device input. A quartz tube with an internal diameter of 3 cm was placed through the nozzles normal to the waveguide wide walls. An atmospheric-pressure stationary discharge was excited by microwaves in a gas flow inside the tube. We used high-purity nitrogen (99.998%), which was introduced into the tube at a flow rate of ~10 L/min. Thus, the quartz tube acted as a plasma-chemical reactor in which microwave plasma was generated. The MV discharge in a continuous wave regime was obtained using a three-phase high-voltage power supply circuit, which allows for the receipt of up to 3 kW of continuous output power from the magnetron. The sample was treated in a plasma flame near the open end of the tube. For oxygen access, a gap of several millimeters was maintained between the open end of the quartz tube and the sample. The treatment time was approximately 1 min.

For microscopic studies, the JCM-6000 (JEOL, Tokyo, Japan) desktop scanning electron microscope (SEM) equipped with an energy dispersive X-ray (EDX) microanalyzer was used. According to SEM (Figure 1b), the average film thickness of Zr on sapphire was 670 nm. X-ray studies were carried out on an X'PERTPRO diffractometer (PANalytical, Almelo, The Netherlands) in the Bragg–Brentano "reflection" geometry using CuK_α radiation (λ = 1.54 Å) with a Ni β-filter. The optical parameters of the films were studied on the SER 850 spectroscopic ellipsometer (SENresearch 4.0 series). To analyze the moisture-resistance properties, the sessile droplet method was used under the following conditions: relative humidity 35–40%, water drop size 5 mm^3. Measurements were performed 30 s after the application to achieve a stable drop state. Methylene Blue (MB) concentrations of

1, 5, and 10 mM were used to determine the effect of MB concentration on the moisture-resistance properties of the solution. Five regions were examined for each sample, and the results were averaged. Raman spectra are recorded on an Ntegra Spectra (NT-MDT) facility (Zelenograd, Russia) at a diode laser wavelength of 532 nm, 20 mW power, and a beam spot of ~5 microns in diameter. A 1 mM solution from MB was prepared to measure SERS spectra. For comparison, pure sapphire substrates and plasma-treated Zr films on sapphire were used.

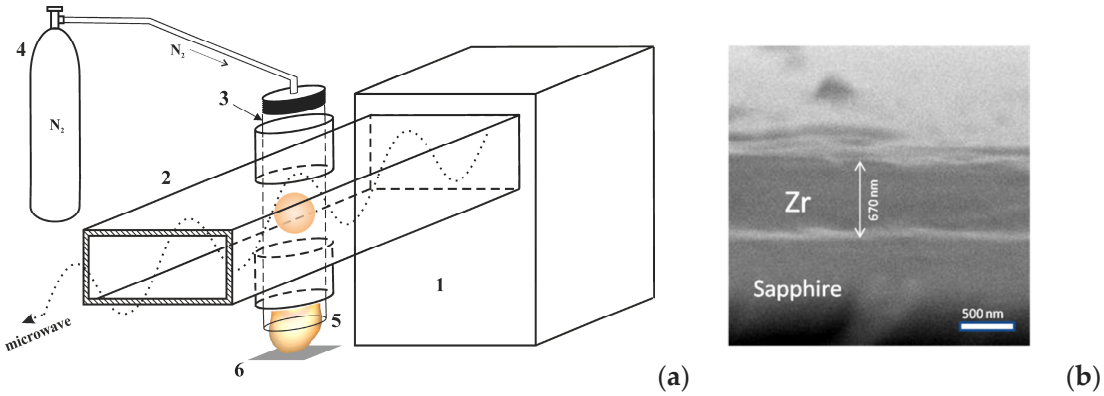

Figure 1. Scheme of the experimental setup with MW plasmatron (**a**): 1—MW unit with a 2.45 GHz magnetron, 2—rectangular waveguide, 3—quartz tube, 4—N_2 gas cylinder, 5—plasma flame, 6—sample. SEM images of Zr/sapphire films (**b**).

3. Results

ZrON Films' Characterization

According to SEM data, a continuous uniform film with a thickness of 670 nm is formed during the deposition of Zr by magnetron sputtering (Figure 1b). Subsequently, the Zr film was treated in nitrogen microwave plasma in the open atmosphere (there was an air inflow). With the power input of approximately 1 kW used in this work, the gas temperature in the near-axial zone of the plasma can be considered 5 kK [15]. A high temperature contributes to the shift of ionization equilibrium in the plasma in favor of increasing ion concentration. For nitrogen plasma, calculations of the temperature dependence of the composition are provided in [24]. At a temperature of 5 kK, the plasma density reaches 10^{19} m^{-3}. However, sample treatment was conducted in the plasma flame behind the quartz tube output at 10–12 cm from the discharge excitation region (waveguide vertical cross-section center). The axial temperature profile along the quartz tube showed a significant decrease, and the expected Zr film treatment temperature at a distance of 10–12 cm from the discharge region was about 1.5 kK. The ionized atoms and molecules of nitrogen are transferred by the gas flow to the open end of the quartz tube and, together with active oxygen drawn from the surrounding atmosphere, form a reactive medium in the Zr film treatment zone.

By selecting the treatment regime of the Zr film (changing the distance from the sample to the open end of the quartz tube) in nitrogen microwave plasma with an oxygen inflow, a structure with heterogeneous morphology was obtained (Figure 2): discrete microbubbles were observed against the background of a continuous film. The nature of microbubbles during plasma treatment is not sufficiently studied, and we can only assume the scheme of their formation. Plasma treatment leads to the formation of active regions as a result of increasing the concentration of free bonds during the implantation of adsorbed impurities and the migration of atoms of the treated materials from the surface inward. Subsequently, the concentration of various defects increases, both in the subsurface layers and in the volume of the material. Judging by the image (Figure 2, insert), a dense bubble wall is initially formed, through which active gases are implanted.

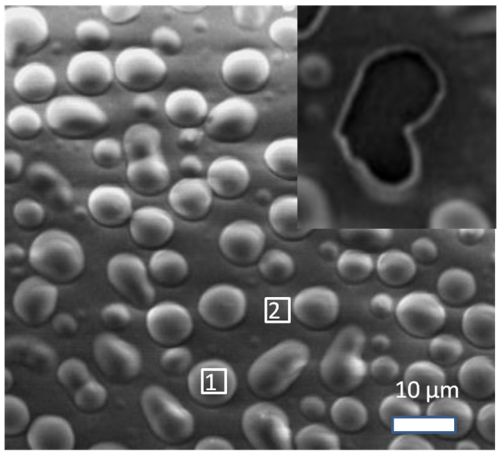

Figure 2. SEM images of the zirconium film on sapphire after treatment in microwave plasma. Symbols: 1—microbubble area; 2—film between microbubbles. Inset: image of an open microbubble.

In the composition of the Zr film after plasma treatment (Table 1), according to EDX data, oxygen predominated, which was likely concentrated both in the film and in the microbubbles. Additionally, the presence of up to 5% nitrogen was observed. The sample after treatment can be classified as zirconium oxynitrides with the general formula ZrON. The study of the surface of the microbubble and the area of the continuous film using Raman spectroscopy (Figure 3) demonstrated the absence of explicit differences. The most intense spectral bands at 185, 197, 226, 342, 354, 387, 483, 510, 542, 565, 625, and 648 cm^{-1} were observed in both curves. The set of bands corresponded to m-ZrO_2 [25], but a significant mixing in the region of higher frequencies (Table 2) corresponding to significant stress [26] was observed. In analyzing the Raman spectrum (Figure 3), bands at 270, 314, 463, and 643 cm^{-1} corresponding to t-ZrO_2 [25] can also be detected. Notably, no significant shifts for the bands of t-ZrO_2 were observed. Moreover, a brightly pronounced band at 424 cm^{-1}, not related to the phases of ZrO_2, was observed in the Raman spectrum. In the Raman spectra of ZrN in this area, two bands are observed: the optical transverse mode (TO) at about 457 cm^{-1} and acoustic modes TA + LA at 407 cm^{-1} [27]. In addition, the band at 231 cm^{-1} probably corresponds to longitudinal acoustic (LA) modes in ZrN [27]. It is likely that significant mechanical stresses can lead to such significant mixings.

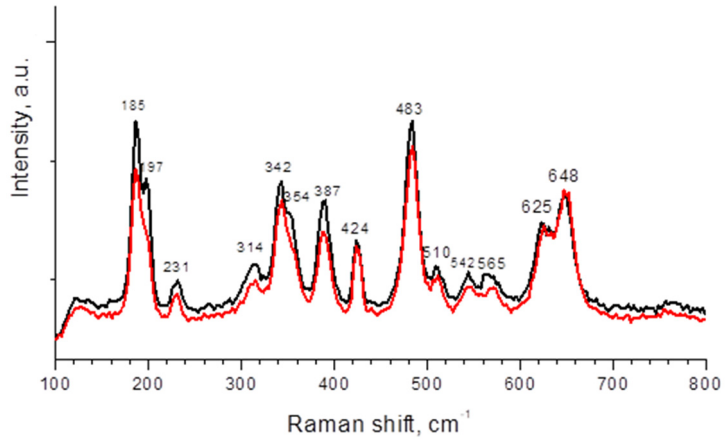

Figure 3. Raman spectra of Zr film after treatment in microwave plasma (m-ZrO_2): black curve—microbubble area; red curve—film between microbubbles.

Table 1. Concentrations (in %) of the components of ZrON thin film.

Element	Zr	O	N
Quantity,%	17.66	77.32	5.02

Table 2. Frequencies (cm^{-1}) of Raman-active phonon modes (A_g and B_g) in monoclinic ZrO_2.

Mode	[25]	This Work
1	103 (Ag)	
2	175 (Bg)	
7	180 (Ag)	185
4	190 (Ag)	197
5	224 (Bg)	
6	313 (Bg)	
7	317 (Ag)	
8	330 (Bg)	342
9	345 (Ag)	354
10	381 (Ag)	387
11	382 (Bg)	
12	466 (Ag)	483
13	489 (Bg)	510
14	533 (Bg)	542
15	548 (Ag)	565
16	601 (Bg)	625
17	631 (Ag)	648
18	748 (Bg)	

According to the XRD data during plasma treatment (Figure 4), a weakly textured film of [111]-ZrON with a structure of t-ZrO_2 (JCPDS # 00-017-0923) is formed. Diffraction peaks were detected at 2θ of 30.2, 35.24, 50.28, 59.4, and 74.1, which can be indexed to the corresponding crystal facets of (111), (200), (220), and (400) of the tetragonal phase of ZrO_2. In addition to the main phase, inclusions of m-ZrO_2 (JCPDS # 00-037-1484) oriented by the planes (−111), (200), (−112), (211), and (400) are observed. The deconvoluted pattern showed (Figure 4b) two peaks corresponding to a minor and major peak of the (−111) plane of monoclinic and (111) plane of tetragonal ZrO_2, respectively.

The lattice parameter d is determined from the Bragg–Wulff equation:

$$2d \times sin(\theta) = \lambda, \quad (1)$$

where θ is the diffraction angle, λ is the wavelength of the used radiation.

Parameters determined by Formula (1) and Figure 4b are d_{111} = 3.13 Å for m-ZrO_2 and d_{111} = 2.98 Å for t-ZrO_2. Experimental stresses were evaluated:

$$\varepsilon = \frac{d_{Teop} - d_{\kappa C\Pi}}{d_{Teop}}, \quad (2)$$

where (d_{exp}) is the change in the experimental interplanar distance relative to the theoretical (d_{theor}).

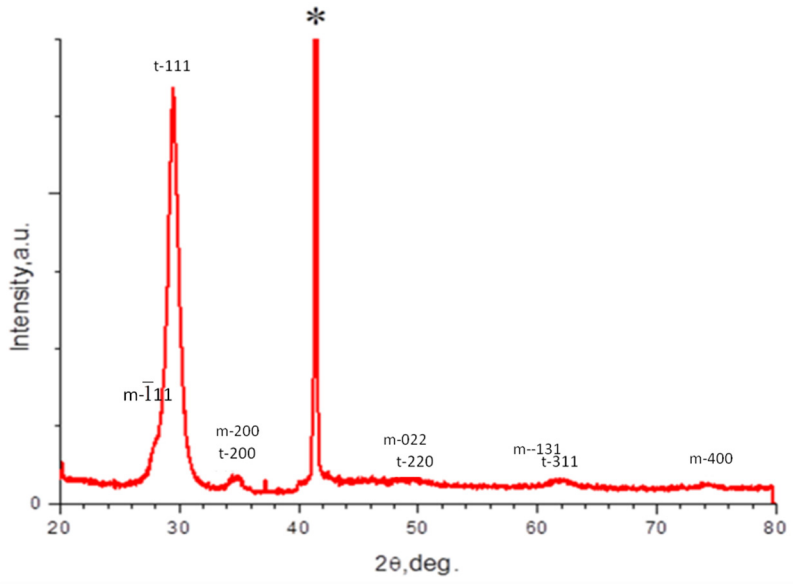

(**a**)

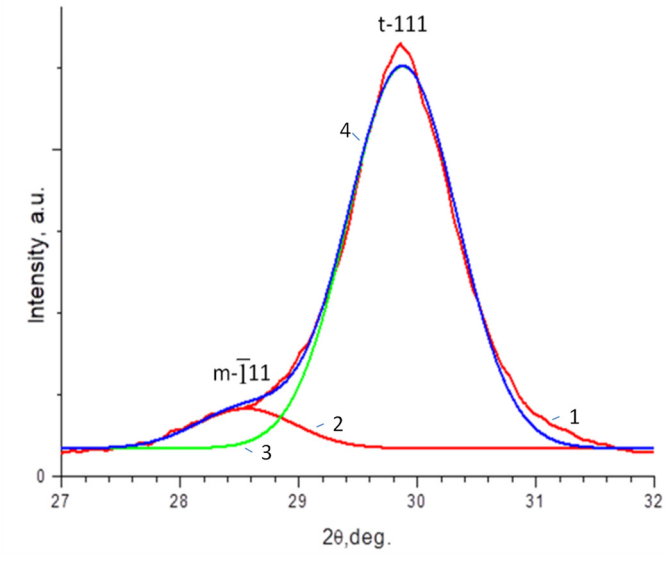

(**b**)

Figure 4. X-ray diffraction pattern of ZrON films (**a**) and deconvoluted (111) peak (**b**). Notation: * sapphire substrate. Symbols: 1—date; 2—fit peak 1; 3—fit peak 2; 4—cumulative fit peak.

According to Formula (2), the experimental stresses were determined to be 0.99% and −0.67%, for the m and t phases, respectively.

The sizes of coherent scattering regions (CSRs) in the samples under study were estimated using the Debye–Scherrer formula:

$$D = \frac{k \cdot \lambda}{\beta \cdot cos\theta}, \quad (3)$$

where D is the average size of CSRs, which can be less than or equal to the grain size; k ~0.9 is the dimensionless particle shape coefficient (Scherrer constant); λ is the wavelength of copper X-ray radiation; β is the width of the reflection at half maximum; θ is the diffraction angle.

The sizes of the crystallites were estimated from Formula (3): 8.3 nm and 7.6 nm for the m-phase and t-phase, respectively.

For the ZrON film, the spectral dependence of the refractive index was measured. Overall, a normal dispersion of the refractive index is observed, typical for the dielectric ZrO_2 [28]. As can be seen from the data in Figure 5, with an increase in light wavelength, the value of the refractive index monotonically decreases, and the dispersion dependence n(λ) appears normal. However, a feature related to plasmonic absorption in the ZrN inclusions is observed in the area of 530 nm, associated with a high density of free electrons within them. Similarly, a strong plasmonic resonance in the area of 500–600 nm was discovered when evaluating the energy loss function in (TiZr)N composition films [29]. The density of free electrons in metal nitrides reaches 10^{21} cm^{-3} [29]. To prevent the spreading and concentration of analyte molecules when studying Raman scattering spectra, the hydrophobicity of the substrate is important. The hydrophobic properties of ZrON films on sapphire were investigated using aqueous MB solutions with concentrations of 1, 5, and 10 mM.

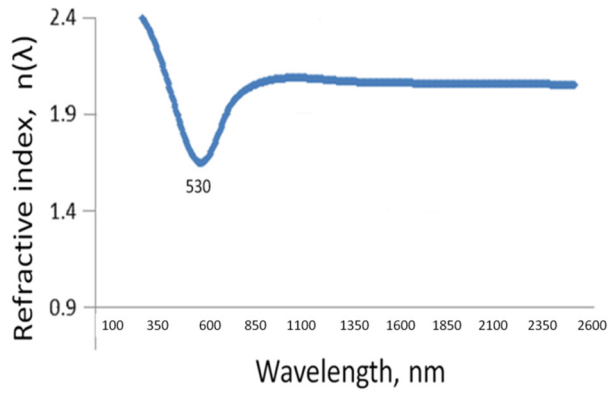

Figure 5. Dispersion of refractive index versus wavelength for the ZrON films.

The contact angle for a droplet (Figure 6) of MB solution was calculated [30]:

$$tg\left(\frac{\vartheta}{2}\right) = \frac{h}{r}, \quad (4)$$

where h is the height of the droplet above the surface, r is the radius of the base of the droplet resting on the ZrO_2 surface. It should be noted that the difference in the contact angles at different MB concentrations in the solution was within error.

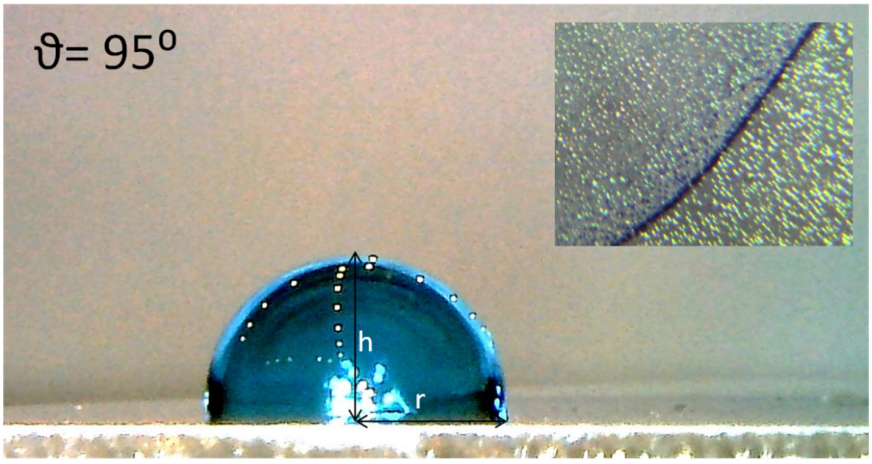

Figure 6. Optical image of the shape of a water droplet of MB solution on the surface of the ZrON film. The drop size is 5 mm^3 and the MB concentration is 10 mM. The edge of the droplet after drying (drying time at room temperature is 5 min).

In accordance with (4), the contact angle was about 95°. According to the accepted classification, surfaces with a contact angle of more than 90° are considered hydrophobic.

It can be observed that the edge of the droplet (Figure 6) did not move after application (the boundary of the droplet after drying is round and the border area is uniform), confirming the hydrophobicity of the ZrON surface.

According to the obtained results, a scheme can be assumed for the formation of the ZrON film during the treatment of the Zr film in nitrogen microwave plasma with an active influx of oxygen from the surrounding atmosphere. The complexity of explaining the processes of micropore formation in the film has been noted earlier. However, the results of Raman spectroscopy of different surface areas demonstrated the homogeneity of the phase composition. Thus, the formation of micropores is not associated with phase formation and the influence of impurities: in particular, nitrogen. Further, it is notable that in the XRD images (Figure 4), covering the entire thickness of the ZrON film, there is a predominant formation of the t-ZrO_2 phase, as well as inclusions of the m-ZrO_2 phase. Calculation according to (2) showed that t-ZrO_2 undergoes tensile stresses, and m-ZrO_2 compressive. The crystallite sizes of both phases, obtained in accordance with (3), are less than 10 nm, confirming the transience of crystallization processes that occurred in the Zr film. At the same time, using the surface-sensitive method of Raman spectroscopy (Figure 3), only the strained phase of m-ZrO_2 was detected, with a small content of t-ZrO_2 inclusions. The presence of the nitride phase is mainly confirmed by EDX methods (Table 1) and the ellipsometry method (Figure 5), which are not surface-sensitive. Moreover, according to EDX data, there is an excess oxygen content in the film. In this case, it is difficult to argue about the substoichiometric content of oxygen, which usually affects the phase processes in ZrO_2 films. Oxygen deficiency may only be observed in the lower layers of the film.

In the initial stage, during the impact of plasma and rapid heating, one can assume the oxidation with the simultaneous process of nitridation of the Zr film. During plasma treatment of the Zr film in an active reactive environment of oxygen and nitrogen, a low-temperature m-phase is first formed, which subsequently transitions to the t-phase. At temperatures above 1000–1100 °C, the m→ t transition processes are likely completed, as the sample spends most of the treatment time in plasma. Upon the rapid removal of the sample (less than 3 s), at the final stage, from the plasma treatment zone, there is a sharp cooling of the sample. Previously [13], it was noted that at this stage, active oxygen, in the absence of access to external active nitrogen, replaces nitrogen in the subsurface layers of the treated film. The nitrogen content profile in the treated films usually peaks in the deeper layers. During cooling below 1100 °C, a reverse t→m extended non-diffusional martensitic transformation occurs, characterized by strong hysteresis [11]. In this regard, speaking about the exact transition temperature is difficult, and it could be lower than the direct m→ t transition. The impurity of nitrogen plays an important role. The t→ m transition, in the absence of impurity, is extended over time and occurs with a volume increase of 4%. Due to the high cooling rate and the presence of nitrogen impurity, the restructuring process is complicated. In the subsurface layers, where there is very little nitrogen, the transition to the monoclinic phase occurs more easily; however, complete relaxation does not occur, and the film remains in a stressed state. Moreover, the presence of a hilly structure prevents surface destruction as a result of the t→ m transition. In deeper layers, nitrogen impurity and oxygen vacancies act as stabilizers of the tetragonal phase and prevent the t→ m transition. The process, which should proceed with an increase in volume, leads to residual tensile stresses in the t-crystallites and compressive stresses in the m-crystallites.

According to [31], only the amorphous ZrO_2 film possessed weak hydrophilicity. During annealing, a polycrystalline t-phase ZrO_2 was formed, which only enhanced hydrophilic properties. The authors associate the enhancement of hydrophilicity with an increase in oxygen vacancy concentration. In [20], it is shown that increasing the roughness

of the t-phase ZrO_2 leads to superhydrophilicity. This phenomenon is described by the Wenzel−Deryagin equation [32]:

$$\cos \theta_r = r \cos \theta, \quad (5)$$

where θ_r—the contact angle of a rough surface, θ—the contact angle of a smooth surface, r—a coefficient that shows how many times the area of a rough surface is greater than that of a smooth one. According to Equation (4), an increase in roughness for wetting bodies leads to a reduction in the contact angle, and for non-wetting bodies to an increase in the contact angle. To increase the hydrophobicity of the t-phase ZrO_2 surface, the use of a hydrophobizing coating is required [20]. As the results show (Figure 6), treating Zr films in nitrogen microwave plasma with the influx of active oxygen forms a ZrON film with hydrophobic properties. The cause of increased hydrophobicity may be due to a low concentration of oxygen vacancies, "hilly" surface topography, and the presence of nitrogen-containing inclusions. Moreover, there are no data on the hydrophilic properties of m-ZrO_2, and the presence of this phase on the surface of ZrON films may play a decisive role.

The SERS properties of the ZrON are presented in Figure 7. The Raman spectra of MB films deposited on ZrON thin film (1) and sapphire (2) were compared. Sapphire was used as a platform without the enhancement effect. The enhancement factor, determined in accordance with [33] from the ratio of the intensities of the 1633 cm^{-1} peak of the MB solution on the ZrON thin film and sapphire at the same MB concentrations, was ~112.

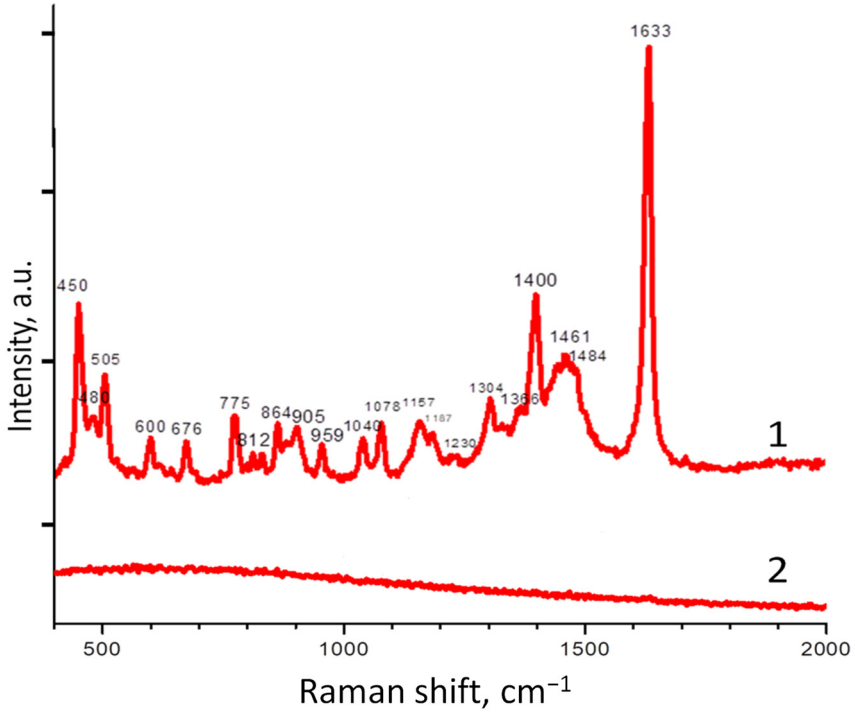

Figure 7. Raman spectra of the MB film deposited on a ZrON thin film (1) and sapphire (2).

It can be observed that the spectral dependence of the Raman scattering intensity peaks of MB on the ZrON substrate corresponds to what was obtained earlier in [34]. There are differences present: high resolution, manifestation of the fine structure of individual intensity peaks. It should be noted (Figure 7) that for some peaks, a shift, enhancement, and separation into components were observed, indicating an SERS effect.

The recorded spectrum is obtained by averaging the signal of all molecules located in the area of the laser spot, and the uniformity of the distribution of substrate surface areas with pronounced plasmonic properties (inclusions of ZrN) contributes to the increase in signal intensity. The hydrophobicity of the ZrON substrate surfaces, together with

the resonant effects on the ZrN inclusions, allows for an increase in the Raman spectrum intensity due to the high concentration of molecules in the scanning area.

4. Conclusions

The features of the formation and morphology of microstructured zirconium oxynitride ZrON films have been investigated, considering structural polymorphism during the influence of atmospheric-pressure microwave nitrogen plasma with the inflow of active oxygen from the surrounding atmosphere. The optical, hydrophobic, and Raman-active properties of ZrON films have been studied. X-ray diffractometry (XRD), scanning electron microscopy (SEM), the ellipsometry method, and Raman spectroscopy, and moisture-resistance properties are used as analytical research methods. It is shown that during the short-term influence of microwave plasma, a morphologically heterogeneous ZrON film can be formed with a set of microhills with a uniform phase composition along the surface. The phase composition of the ZrON surface corresponds to the monoclinic structure of ZrO_2. Predominantly, a tetragonal structure of ZrO_2, as well as inclusions of the monoclinic structure of ZrO_2, are observed in the film volume. A mechanism for the formation of the ZrON film, considering polymorphism and phase transitions, is proposed. The optical properties of ZrON films are determined by both the dielectric phase of ZrO_2 and the inclusions of the highly conductive phase of ZrN. A combination of such factors as developed micro-relief, the monoclinic structure of the surface, and the inclusions of the nitride phase enhance the hydrophobic properties of the ZrON film surfaces. Using MB as an example, it is shown that the hydrophobicity of the surface and resonant effects on the ZrN inclusions allow for the enhancement of the Raman spectrum intensity due to the high concentration of analyte molecules in the scanning area.

Author Contributions: Conceptualization, A.M., S.A. and M.G.; methodology, A.M. and M.G.; validation, A.M. and M.G.; formal analysis, V.K.; investigation, S.A. and A.M.; resources, A.M., M.G., S.A. and V.K.; writing, A.M.; writing—review and editing, A.M.; visualization, A.M.; supervision, A.M., M.G. and V.K.; project administration, A.M. and V.K.; funding acquisition, A.M. and V.K. All authors have read and agreed to the published version of the manuscript.

Funding: This research was performed in the frame of a grant from the Russian Science Foundation (project No. 21-79-30062 in part sample making by microwave plasmatron), and in the frame of state assignments of the Ministry of Science and Higher Education of the Russian Federation for FSRC "Crystallography and Photonics" RAS (in part X-ray diffractometry (XRD), scanning electron microscopy (SEM) and Raman spectroscopy studies of samples), Joint Institute for High Temperatures, Russian Academy of Sciences (State Assignment No. 075-01129-23-00, in the part ellipsometry method and moisture-resistance properties studies of samples).

Data Availability Statement: The data presented in this study are available on request from the corresponding author.

Acknowledgments: The authors are grateful to R.G. Valeev (Center for Physical and Physico-Chemical Methods of Analysis, Study of the Properties, and Characteristics of Surfaces, Nanostructures, Materials, and Products, UdmFRC Ural Branch of the Russian Academy of Sciences) for their help in the study of samples.

Conflicts of Interest: The authors declare no conflict of interest.

References

1. McCauley, J.W.; Patel, P.; Chen, M.; Gilde, G.; Strassburger, E.; Paliwal, B.; Ramesh, K.T.; Dandekar, D.P. AlON: A brief history of its emergence and evolution. *J. Eur. Ceram. Soc.* **2009**, *29*, 223–236. [CrossRef]
2. Corbin, N.D. Aluminum oxynitride spinel: A review. *J. Eur. Ceram. Soc.* **1989**, *5*, 143–154. [CrossRef]
3. Arunachalam, M.; Yun, G.; Ahn, K. Unique photoelectrochemical behavior of TiO_2 nanorods wrapped with novel titanium Oxy-Nitride (TiOxNy) nanoparticles. *Int. J. Hydrog. Energy* **2018**, *43*, 16458–16467. [CrossRef]
4. Chisaka, M.; Ishihara, A.; Ota, K.; Muramoto, H. Electrochimica Acta Synthesis of carbon-supported titanium oxynitride nanoparticles as cathode catalyst for polymer electrolyte fuel cells. *Electrochim. Acta* **2013**, *113*, 735–740. [CrossRef]

5. Ohashi, M.; Kanzaki, S.; Tabata, H. Processing, Mechanical Properties, and Oxidation Behavior of Silicon Oxynitride Ceramics. *J. Am. Ceram. Soc.* **1991**, *74*, 109–114. [CrossRef]
6. Ohashi, M.; Kanzaki, S.; Tabata, H. Effect of additives on some properties of silicon oxynitride ceramics. *J. Mater. Sci.* **1991**, *26*, 2608–2614. [CrossRef]
7. Kharitonov, A.V.; Sergey, S.K. Tunable optical materials for multi-resonant plasmonics: From TiN to TiON. *Opt. Mater. Express* **2020**, *10*, 513–531. [CrossRef]
8. Xin, Y.; Xu, T.; Wang, Y.; Luo, P.; Li, W.; Kang, B.; Mei, B.; Jing, W. Effect of ZrO_2 Content on Microstructure Evolution and Sintering Properties of $(Tb_{0.7}Lu_{0.3})_2O_3$ Magneto-Optic Transparent Ceramics. *Magnetochemistry* **2022**, *8*, 175. [CrossRef]
9. Patsalas, P. Zirconium nitride: A viable candidate for photonics and plasmonics? *Thin Solid Film.* **2019**, *688*, 137438. [CrossRef]
10. Kozlovskiy, A.L.; Alin, M.; Borgekov, D.B. Study of Polymorphic Transformation Processes and Their Influence in Polycrystalline ZrO_2 Ceramics upon Irradiation with Heavy Ions. *Ceramics* **2023**, *6*, 686–706. [CrossRef]
11. Kulyk, V.; Duriagina, Z.; Vasyliv, B.; Vavrukh, V.; Kovbasiuk, T.; Lyutyy, P.; Vira, V. The Effect of Sintering Temperature on the Phase Composition, Microstructure, and Mechanical Properties of Yttria-Stabilized Zirconia. *Materials* **2022**, *15*, 2707. [CrossRef]
12. Muslimov, A.E.; Gadzhiev, M.K.; Kanevsky, V.M. Influence of Plasma Treatment Parameters on the Structural-Phase Composition, Hardness, Moisture-Resistance, and Raman-Enhancement Properties of Nitrogen-Containing Titanium Dioxide. *Materials* **2022**, *15*, 8514. [CrossRef] [PubMed]
13. Muslimov, A.; Orudzhev, F.; Gadzhiev, M.; Selimov, D.; Tyuftyaev, A.; Kanevsky, V. Facile Synthesis of Ti/TiN/TiON/TiO_2 Composite Particles for Plasmon-Enhanced Solar Photocatalytic Decomposition of Methylene Blue. *Coatings* **2022**, *12*, 1741. [CrossRef]
14. Dombrovskii, L.A.; Isakaev, E.H.; Senchenko, V.N.; Chinnov, V.F.; Scherbakov, V.V. Efficiency of particle acceleration, heating, and melting in high-enthalpy plasma jets. *High Temp.* **2012**, *50*, 145–153. [CrossRef]
15. Chen, C.J.; Li, S.Z. Spectroscopic measurement of plasma gas temperature of the atmospheric-pressure microwave induced nitrogen plasma torch. *Plasma Sources Sci. Technol.* **2015**, *24*, 035017. [CrossRef]
16. Wang, J.; Lin, W.; Cao, E.; Xu, X.; Liang, W.; Zhang, X. Surface Plasmon Resonance Sensors on Raman and Fluorescence Spectroscopy. *Sensors* **2017**, *17*, 2719. [CrossRef]
17. Moldovan, R.; Toma, V.; Iacob, B.-C.; Știufiuc, R.I.; Bodoki, E. Off-Resonance Gold Nanobone Films at Liquid Interface for SERS Applications. *Sensors* **2022**, *22*, 236. [CrossRef]
18. Yasui, T.; Hayashi, K.; Fukumoto, M. Behaviors of Micro-Arcs, Bubbles, and Coating Growth during Plasma Electrolytic Oxidation of β-Titanium Alloy. *Materials* **2023**, *16*, 360. [CrossRef]
19. Xu, L.; Ma, J.; Wei, G.; Gu, C.; Jiang, T. Improved surface-enhanced Raman scattering performance enabled by hydrophilic-hydrophobic piezoelectric PVDF-silver substrate. *Sens. Actuators B* **2022**, *370*, 132431. [CrossRef]
20. Duan, Z.; Luo, D.; Liu, Z.; Zhao, Z.; Zhao, M.; Zhang, J.; Zhao, G. Patterning ZrO 2 films surface: Superhydrophilic and superhydrophobic properties. *Ceram. Int.* **2017**, *43*, 5089–5094. [CrossRef]
21. Antonov, D.V.; Islamova, A.G.; Strizhak, P.A. Hydrophilic and Hydrophobic Surfaces: Features of Interaction with Liquid Drops. *Materials* **2023**, *16*, 5932. [CrossRef] [PubMed]
22. Tikhonov, V.N.; Aleshin, S.N.; Ivanov, I.A.; Tikhonov, A.V. The low-cost microwave plasma sources for science and industry applications. *J. Phys. Conf. Ser.* **2017**, *927*, 012067. [CrossRef]
23. Chepelev, V.M.; Chistolinov, A.V.; Khromov, M.A.; Antipov, S.N.; Gadzhiev, M.K. Thermocouple and electric probe measurements in a cold atmospheric-pressure microwave plasma jet. *J. Phys. Conf. Ser.* **2020**, *1556*, 012091. [CrossRef]
24. Rahman, M.Z.; Mynuddin, M. Kinetic Modelling of Atmospheric Pressure Nitrogen Plasma. *Am. J. Mod. Phys.* **2018**, *7*, 185–193.
25. Zhao, X.; Vanderbilt, D. Phonons and lattice dielectric properties of zirconia. *Phys. Rev. B* **2002**, *65*, 075105. [CrossRef]
26. Efaw, C.M.; Vandegrift, J.L.; Reynolds, M.; McMurdie, S.; Jaques, B.J.; Hu, H.; Hui, X.; Hurley, M.F. Characterization of zirconium oxides part I: Raman mapping and spectral feature analysis. *Nucl. Mater. Energy* **2019**, *21*, 100707. [CrossRef]
27. Kuznetsov, K.B.; Kovalev, I.A.; Nechaev, A.N.; Ogarkov, A.I.; Shevtsov, S.V.; Chernyavskii, A.S.; Solntsev, K.A. Stability of the structure of compact zirconium nitride ceramics to irradiation with high-energy xenon ions. *Inorg. Mater.* **2016**, *52*, 1235–1239. [CrossRef]
28. Kruchinin, V.N.; Aliev, V.S.; Gerasimova, A.K.; Gritsenko, V.A. Optical properties of nonstoichiometric ZrO x according to spectroellipsometry data. *Opt. Spectrosc.* **2016**, *121*, 241–245. [CrossRef]
29. Chen, L.; Ran, Y.; Jiang, Z.; Li, Y.; Wang, Z. Structural, Compositional, and Plasmonic Characteristics of Ti–Zr Ternary Nitride Thin Films Tuned by the Nitrogen Flow Ratio in Magnetron Sputtering. *Nanomaterials* **2020**, *10*, 829. [CrossRef]
30. Yuan, Y.; Lee, T.R. *Surface Science Techniques*; Bracco, G., Holst, B., Eds.; Springer Series in Surface Sciences; Springer: Berlin/Heidelberg, Germany, 2013; Volume 51, pp. 3–34.
31. Méndez-López, A.; Zelaya-Ángel, O.; Toledano-Ayala, M.; Torres-Pacheco, I.; Pérez-Robles, J.F.; Acosta-Silva, Y.J. The Influence of Annealing Temperature on the Structural and Optical Properties of ZrO_2 Thin Films and How Affects the Hydrophilicity. *Crystals* **2020**, *10*, 454. [CrossRef]
32. Belov, N.A.; Alentiev, A.Y.; Bogdanova, Y.G.; Vdovichenko, A.Y.; Pashkevich, D.S. Direct Fluorination as Method of Improvement of Operational Properties of Polymeric Materials. *Polymers* **2020**, *12*, 2836. [CrossRef] [PubMed]

33. Le Ru, E.C.; Blackie, E.; Meyer, M.; Etchegoin, P.G. Etchegoin Surface Enhancedment Raman Scattering Enhacement Factors: A Comprehensive Study. *J. Phys. Chem. C* **2007**, *111*, 13794–13803. [CrossRef]
34. Li, C.; Huang, Y.; Lai, K.; Rasco, B.A.; Fan, Y. Analysis of trace methylene blue in fish muscles using ultra-sensitive surface-enhanced Raman spectroscopy. *Food Control.* **2016**, *65*, 99–105. [CrossRef]